Cluster synchronization in networks of identical oscillators with α-function pulse coupling

Bolun Chen,[1] Jan R. Engelbrecht,[1] and Renato Mirollo[2]
[1]*Department of Physics, Boston College, Chestnut Hill, Massachusetts 02467, USA*
[2]*Department of Mathematics, Boston College, Chestnut Hill, Massachusetts 02467, USA*
(Received 1 December 2015; revised manuscript received 20 November 2016; published 9 February 2017)

We study a network of N identical leaky integrate-and-fire model neurons coupled by α-function pulses, weighted by a coupling parameter K. Studies of the dynamics of this system have mostly focused on the stability of the fully synchronized and the fully asynchronous splay states, which naturally depends on the sign of K, i.e., excitation vs inhibition. We find that there is also a rich set of attractors consisting of clusters of fully synchronized oscillators, such as fixed $(N-1,1)$ states, which have synchronized clusters of sizes $N-1$ and 1, as well as splay states of clusters with equal sizes greater than 1. Additionally, we find limit cycles that clarify the stability of previously observed quasiperiodic behavior. Our framework exploits the neutrality of the dynamics for $K=0$ which allows us to implement a dimensional reduction strategy that simplifies the dynamics to a continuous flow on a codimension 3 subspace with the sign of K determining the flow direction. This reduction framework naturally incorporates a hierarchy of partially synchronized subspaces in which the new attracting states lie. Using high-precision numerical simulations, we describe completely the sequence of bifurcations and the stability of all fixed points and limit cycles for $N=2$–4. The set of possible attracting states can be used to distinguish different classes of neuron models. For instance from our previous work [Chaos **24**, 013114 (2014)] we know that of the types of partially synchronized states discussed here, only the $(N-1,1)$ states can be stable in systems of identical coupled sinusoidal (i.e., Kuramoto type) oscillators, such as θ-neuron models. Upon introducing a small variation in individual neuron parameters, the attracting fixed points we discuss here generalize to equivalent fixed points in which neurons need not fire coincidently.

DOI: 10.1103/PhysRevE.95.022207

I. INTRODUCTION

Pulse-coupled oscillator networks are oscillator networks in which the oscillators do not communicate continuously; instead, the oscillators each evolve completely independently of each other, except when an oscillator reaches some threshold level and then undergoes a "firing event." When an oscillator fires, it then emits a pulse, which in some way alters the evolution of the other oscillators in the network. Pulse-coupled oscillator networks are natural models for a variety of systems in nature, such as the cardiac pacemaker, neural networks, and most famously, swarms of fireflies that flash in unison. Beginning with the pioneering work of Winfree [1] and Peskin [2] in the 1960s and 1970s, these systems have been studied extensively; it is impossible to summarize in a short discussion all the important work in the vast literature on this topic. We are mainly interested in the subclass of systems in which the individual oscillators have identical dynamics and affect each other in the same way; in this case the oscillator network has "all-to-all" coupling. All-to-all models are a highly idealized class since they ignore the possible effects of network architecture, but they are often analytically tractable due to their inherent symmetries and hence have received particular attention in the work on pulse-coupled networks.

All-to-all networks of identical oscillators have the (sometimes) desirable property that synchrony cannot be broken; in other words, the sync states, which we define as states such that all oscillators have the same phase, are preserved by the dynamics. This is because when the oscillators simultaneously reach threshold and fire, the effect of the firings is the same on each oscillator in the network, so they all remain in sync. However, this does not imply that synchrony is stable; this depends sensitively on the form of the coupling. For example, Mirollo and Strogatz [3] proved that synchrony is stable in all-to-all networks with excitatory δ-function coupling (when one oscillator fires, all others advance discontinuously by the same amount up to but not exceeding their thresholds). But in networks with continuous pulses, synchrony is not always stable as was first shown by Abbott and van Vreeswijk [4] for leaky integrate-and-fire (LIF) networks with excitatory α-function coupling. Note that an α-function pulse attains its maximum magnitude at time $\tau=1/\alpha$ after the onset of the pulse, so there is a delay inherent with the effect of α-function coupling unlike the case of δ-function coupling.

Synchrony is of course a highly symmetric configuration of states; not surprisingly, all-to-all networks have a variety of other states which are symmetric in the sense that they are invariant under some permutations of the oscillators and which may or may not be dynamically stable. At the other extreme from synchrony are splay states in which the oscillators all evolve according to the same periodic function but equally staggered in phase. Splay states can be stable, for example, in all-to-all networks with inhibitory δ-function coupling [5]. There are many studies of splay states and their stability [4,6–10]. The stability of splay states can often be analyzed in the continuum limit as the number of oscillators $N\to\infty$ since the distribution of the oscillator phases becomes stationary for splay states in this limit. Olmi and co-workers [9,11] have thoroughly analyzed this problem for networks with δ-function coupling using a perturbative approach in $1/N$ to study the stability of splay states. Of course, the analysis of splay states in continuum limit models sheds little light on their behavior for small N networks, which is the primary focus of this paper.

It may be tempting to conclude that the dichotomy between sync and splay states is the whole story, but this is far from the case. All-to-all networks of identical pulse-coupled oscillators have a variety of partially synchronized states: If $N = n_1 + n_2 + \cdots + n_M$ is any partition of N, then the network has partially synchronized states with n_i oscillators in each of the M synchronized clusters. And partially synchronized states with synchronized clusters of different sizes can also be stable. For example, we will see systems with $N = 4$ oscillators which have stable partially synchronized states with a (3,1) configuration (i.e., a cluster of three oscillators in sync, the remaining one out of phase with the cluster of three).

For inhibitive coupling, we also find stable sates consisting of M distinct equally sized clusters ($n_i = N/M$) in a splay configuration, where $N = n_i \times M$. For $N = 4$ and 6 we find stable (2,2), (2,2,2), and (3,3) partially synchronized splay states. Note that for systems of identical coupled sinusoidal (i.e., Kuramoto type) oscillators, $(N-1,1)$ states are the only possible stable asynchronous configurations [12]; this is a consequence of the invariance under the action of the Möbius group on the state space. The existence of stable (2,2) states in the case of pulse-coupled networks implies that the dynamics of these networks cannot be replicated by Kuramoto networks. For inhibitive coupling and $N < 7$, the only stable partially synchronized states are $(N-1,1)$ or equal-cluster splay configurations. In contrast, using numerical simulations for 100 oscillators, van Vreeswijk found [7] clustered states which were not equally sized in a splay configuration nor of the $(N-1,1)$ variety.

The organization of this paper is as follows: we begin by setting up a standard model of N identical LIF neurons with α-function pulse coupling, which has an $(N+2)$-dimensional state space. We reduce the dynamics down one dimension by constructing a return map that relates consecutive states right after a complete cycle of N firing events. We accomplish a further reduction in dimension by assuming that the coupling is small; in the limit of weak coupling the discrete dynamics of the firing event map can be approximated by the continuous dynamics of an associated ordinary differential equation (ODE) model of lower dimension (one dimension lower for exponential pulses, two dimensions lower for α-function pulses). So, for example, the system with $N = 3$ oscillators and α-function pulses, which has a five-dimensional state space, can be reduced to a two-dimensional flow. We investigate the dynamics of our reduced systems numerically and map out in parameter space some of the different stable configurations we observe. These include, not surprisingly, stable sync and splay states but also a variety of partially synchronized states and limit cycles (LCs), including (2,2) configurations as well as the (3,1) configurations mentioned above. We conclude with a discussion of our findings and future directions for this work.

II. MODEL

We begin by setting up a classic all-to-all LIF network as described in Ref. [4]. A state of this model is an $(N+2)$-dimensional vector $(\mathbf{x},s,b) = (x_1,\ldots,x_N,s,b)$, where $x_i \leqslant 1$. Here x_i's represent the voltages of the N individual oscillators, and s and b are auxiliary variables that determine a global field through which the oscillators are coupled. Provided that all $x_i < 1$, the state variables x_i, s, and b evolve according to the equations,

$$\begin{aligned} \dot{x}_i &= a - x_i + Ks, \qquad i = 1,\ldots,N, \\ \dot{s} &= \alpha(-s+b), \quad \dot{b} = -\alpha b, \end{aligned} \tag{1}$$

where $a > 1$, $\alpha > 0$, and K are constant parameters. Since $a > 1$ we are modeling suprathreshold LIF neurons, which are equivalent to phase rotators because they fire periodically in the absence of coupling. The parameter α determines the shape of the pulses emitted when oscillators fire, and K is a coupling constant (which can be any real number). We assign weights $w_i > 0$ to the oscillators and assume $\sum w_i = 1$; $w_i = 1/N$ when the N oscillators are weighted equally. The rationale for introducing the weights w_i is that if an initial condition for the equal weight model with N oscillators consists of $M < N$ clusters of synchronized oscillators, then this partial synchrony is never broken, and the evolution of this state reduces to a model for M oscillators but with different weights if the clusters are not all equal in size.

Firings occur when one or more of the variables x_i reach the threshold $x = 1$; when this happens we reset x_i to 0, b is augmented by $w_i\alpha$, and s is unchanged. If oscillator i fires at time t_0, the global field $s(t)$ is augmented by the function $w_i\phi(t-t_0)$ where $\phi(t)$ is the α-function pulse defined by

$$\phi(t) = \alpha^2 t e^{-\alpha t}.$$

[The parameter α determines the time $\tau = 1/\alpha$ at which $\phi(t)$ attains its maximum value.] Between firings, $s(t)$ obeys the ODE,

$$\ddot{s} + 2\alpha\dot{s} + \alpha^2 s = 0,$$

so $s(t)$ has the form $(A+Bt)e^{-\alpha t}$ and hence would decay to 0 in the absence of firings. Notice that since $a > 1$, firings will eventually occur; if not, then $s(t)$ would decay to 0, but then each oscillator reaches threshold in finite time.

III. DIMENSIONAL REDUCTIONS

Following Zillmer *et al.* [8], we transform the continuously evolving system described above to a discrete dynamical system on a state space one dimension lower by use of a return map. The idea is to look at a snapshot of the model immediately after one or more of the oscillators has fired and reset to 0. Note that it is possible for the oscillator variables x_i to drop below $x = 0$; indeed, this can happen for large negative K, even if we assume our initial condition has all $x_i > 0$. However, if we define the width of a state by $\delta = \max x_i - \min x_i$, then we claim that eventually δ will drop below and remain less than 1. To see this, observe that between firings, δ satisfies the ODE $\dot{\delta} = -\delta$ and hence decays exponentially between firings. If $\delta \geqslant 1$ when a firing occurs, then we must have some $x_i \leqslant 0$, and hence δ does not increase due to this firing; this implies that we must eventually obtain $\delta < 1$. And once a state has $\delta < 1$, this condition holds for the subsequent evolution of that state. So we may as well only consider postfiring states with all $x_i \geqslant 0$.

If we assume that the Nth oscillator has fired and reset, then we can take as our state space set X of vectors $(\mathbf{x},s,b)$ with

$$\mathbf{x} = (x_1,\ldots,x_{N-1}), \qquad 0 \leqslant x_i < 1. \tag{2}$$

If we identify 0 and 1, then X is just the product of the $(N-1)$-fold torus T^{N-1} with $\mathbb{R}^2$. Let $F(\mathbf{x},s,b) \in X$ denote the evolution of state $(\mathbf{x},s,b) \in X$ after one complete cycle of N firings (each oscillator fires once). The discrete dynamics of the return map F completely capture the continuous dynamics of the original model on a state space of dimension $N+1$, one less than the original. In the case of equal weights w_i, the state space X can be partitioned into $(N-1)!$ fundamental domains, which are the open sets in which the variables $x_1,\ldots,x_{N-1}$ are distinct and have the same ordering; these fundamental domains are each invariant under F and have identical dynamics, so we can restrict our attention to any one of these domains, say X_0 given by

$$0 \leqslant x_{N-1} \leqslant \cdots \leqslant x_1 < 1.$$

The boundaries of the fundamental domains consist of states with at least one cluster of two or more identical x_i's and are invariant under the dynamics. The dynamics on the boundary components can be viewed as systems with fewer oscillators but possibly unequal weights w_i.

Our approach differs from that of Zillmer *et al.* [8] where only the case of equal weights w_i is considered. They describe the dynamics by an "event-driven map" that is the result of a *single*-firing event. In their formulation the states can be taken as configurations of points $0 \leqslant x_{N-1} \leqslant \cdots \leqslant x_1 \leqslant 1$ together with a vector (s,b). Their firing map is given by taking the new configuration of points after oscillator No. 1 fires and resets to zero and then shifting each index down by one. An advantage of their formulation is that the fixed points of the single-firing map are exactly the splay states. A disadvantage is that the single-firing map is discontinuous at partially synchronized states. In our formulation the return map F is continuous on the full state space and has a richer set of fixed points, including both the sync and the splay states, various types of partially synchronized states, and higher order periodic points of the single-firing map.

We next explain how to accomplish an additional reduction of two more dimensions in the limit of small coupling $K \to 0$. Consider the system in the case of $K = 0$; then the equations for the oscillator states x_i are uncoupled and independent of the variables s and b, although the evolution of s and b still depends on the firing times of the oscillators. Suppose $(\mathbf{x},s,b) \in X$; then, after N firings, $\mathbf{x}$ is unchanged, so we have

$$F(\mathbf{x},s,b) = (\mathbf{x},s',b')$$

for some $s',b' \in \mathbb{R}$. We can describe the evolution of the variables s and b as follows: Let s_0 and b_0 be their initial values, and let s_j,b_j be their values after the jth firing, $j = 1,\ldots,N$. Assume the oscillators fire in order $1,2,\ldots,N$ and let $t_1,\ldots,t_N$ be the times between consecutive firings; then

$$t_1 + \cdots + t_N = T,$$

where $T > 0$ is the time for each oscillator to go from reset $x = 0$ to threshold $x = 1$. Then we have

$$\begin{pmatrix} s_j \\ b_j \end{pmatrix} = \exp(t_j A)\begin{pmatrix} s_{j-1} \\ b_{j-1} \end{pmatrix} + \begin{pmatrix} 0 \\ w_j\alpha, \end{pmatrix}$$

where $j = 1,\ldots,N$ and A is the matrix governing the evolution of s and b,

$$A = \alpha\begin{pmatrix} -1 & 1 \\ 0 & -1 \end{pmatrix}.$$

Inductively, we see that we can express

$$\begin{pmatrix} s_N \\ b_N \end{pmatrix} = \exp(TA)\begin{pmatrix} s_0 \\ b_0 \end{pmatrix} + \mathbf{v}(\mathbf{x}),$$

where the vector $\mathbf{v}(\mathbf{x})$ depends on α, the weights w_i, and the vector $\mathbf{x}$ through the interspike times t_j. Since A has repeated eigenvalue $-\alpha < 0$, this iteration converges exponentially to the unique fixed point given by

$$\begin{pmatrix} s_0(\mathbf{x}) \\ b_0(\mathbf{x}) \end{pmatrix} = [I - \exp(TA)]^{-1}\mathbf{v}(\mathbf{x}).$$

The codimension 2 submanifold $\tilde{X}_0$ given by states $[\mathbf{x},s_0(\mathbf{x}),b_0(\mathbf{x})]$ is invariant and attracting in the full state space X for the system with $K = 0$.

Now suppose $K \neq 0$; then for K sufficiently close to 0, the system will continue to have a codimension 2 invariant and attracting subspace $\tilde{X}_K$, which we can parametrize in the form

$$(\mathbf{x},s_K(\mathbf{x}),b_K(\mathbf{x})), \qquad \mathbf{x} = (x_i), \qquad 0 \leqslant x_i < 1,$$

with $i = 1,\ldots,N-1$. The dynamics of F on $\tilde{X}_K$ are completely determined by the dynamics in the vector $\mathbf{x}$ and reduce to the identity map for $K = 0$. Let us denote temporarily the return map for a given K by F_K and expand at $K = 0$ to first order in K on the full state space X,

$$F_K(\mathbf{x},s,b) \approx F_0(\mathbf{x},s,b) + KG(\mathbf{x},s,b)$$

for some function G on X. Let us also expand the functions s_K and b_K,

$$s_K(\mathbf{x}) \approx s_0(\mathbf{x}) + Ku(\mathbf{x}),$$
$$b_K(\mathbf{x}) \approx b_0(\mathbf{x}) + Kv(\mathbf{x})$$

for some functions u and v on T^{N-1}. Then on the reduced state space $\tilde{X}_K$ we have an expansion to first order in K,

$$\begin{aligned} &F_K(\mathbf{x},s_K(\mathbf{x}),b_K(\mathbf{x})) \\ &\quad\approx F_0(\mathbf{x},s_0(\mathbf{x}) + Ku(\mathbf{x}),b_0(\mathbf{x}) + Kv(\mathbf{x})) \\ &\qquad + KG(\mathbf{x},s_0(\mathbf{x}),b_0(\mathbf{x})). \end{aligned}$$

The dynamics in $\mathbf{x}$ on $\tilde{X}_K$ are given by the first component of $F_K(\mathbf{x},s_K(\mathbf{x}),b_K(\mathbf{x}))$. The first component of $F_0(\mathbf{x},s_0(\mathbf{x}) + Ku(\mathbf{x}),b_0(\mathbf{x}) + Kv(\mathbf{x}))$ is just $\mathbf{x}$, which has no K dependence. So we see that, to first order in K, the dynamics in $\mathbf{x}$ on $\tilde{X}_K$ are given by a function of the form

$$\mathbf{x} \mapsto \mathbf{x} + Kg(\mathbf{x}),$$

where g is just the first component of $G(\mathbf{x},s_0(\mathbf{x}),b_0(\mathbf{x}))$. Notice that, if we instead expand F_K on $\tilde{X}_0$, namely, expand $F_K(\mathbf{x},s_0(\mathbf{x}),b_0(\mathbf{x}))$ to first order in K, we get the same first order expansion! In other words, if we use the approximate values $s_0(\mathbf{x})$ and $b_0(\mathbf{x})$ instead of the correct values $s_K(\mathbf{x})$ and $b_K(\mathbf{x})$ to determine the dynamics in $\mathbf{x}$ along the invariant subspace $\tilde{X}_K$, we will be correct to first order in K.

So we see that, in the $K \to 0$ limit, the dynamics of our model reduce to an iteration of the form $\mathbf{x} \mapsto \mathbf{x} + Kg(\mathbf{x})$,

where g is a function on the torus T^{N-1}. This discrete iteration is just Euler's method for $\dot{\mathbf{x}} = \pm g(\mathbf{x})$ on T^{N-1} with time step $|K|$, so we ultimately see that, in the $K \to 0$ limit, the dynamics of our original system reduce to the continuous dynamical system $\dot{\mathbf{x}} = \pm g(\mathbf{x})$ on T^{N-1}, where $\pm$ is the sign of K (the observation that the dynamics reduce to a continuous system in the $K \to 0$ limit can also be found in Refs. [13,14]. Thus we obtain a reduction of three dimensions from the original model. The function $g(\mathbf{x})$ depends only on the parameters a and α, not on K. Observe that, in the $K \to 0$ limit, the dynamics for excitatory ($K > 0$) and inhibitory ($K < 0$) couplings are identical under time reversal.

IV. ATTRACTORS AND BIFURCATIONS

In this section we describe the dynamics of the reduced model $\dot{\mathbf{x}} = \pm g(\mathbf{x})$ on T^{N-1}, focusing on the stability and bifurcations of fixed points and limit cycles as a function of the parameter α. Our results are based on numerical solutions of the original discrete system for small $|K|$ and values of a slightly above the threshold 1 (such as $a = 1.05$).

We start by reviewing the case of two identical coupled oscillators ($N = 2$ and $w_1 = w_2$) studied in the classic paper of van Vreeswijk *et al.* [6]. The dynamics reduce to a flow on the unit circle T^1. For small α the flow has the simplest possible fixed point structure, namely, one sink and one source. For $K \to 0^-$ the stable fixed point is the synchronized state $x_1 = 0$, and the unstable fixed point is the splay state. [Note that the splay fixed point is not $x_1 = \frac{1}{2}$ in this representation since $\dot{x}$ is not constant. For $K = 0$ each oscillator fires with period $T = \ln[a/(a-1)]$ so the interspike period for a splay state is $T/2 = \ln\sqrt{a/(a-1)}$. This gives $x_1 = a - \sqrt{a(a-1)} > \frac{1}{2}$ in the $K \to 0$ limit.] As discussed in Ref. [6] the splay fixed point undergoes a pitchfork bifurcation at a threshold value of α_c. The two states born at this bifurcation are equivalent in the sense that each maps to the other under a single firing (and exchange of indices). For $\alpha > \alpha_c$ both sync and splay states are stable for $K \to 0^-$. As α increases further the basin of attraction of the splay grows, approaching all of T^1 for large α.

For $K \to 0^+$ the flow direction is reversed, resulting in a stable splay and an unstable sync state for small α. The two states born at the pitchfork bifurcation (PF) of the splay state are now stable and converge to the sync state in the large α limit. The attractors and bifurcations in the $K \to 0$ limit for $N = 2$, $w_1 = w_2$ and fixed a are shown in Fig. 1.

Our analysis for $N > 2$ will place considerable emphasis on partially synchronized subspaces of T^{N-1}, which lie in the codimension 1 boundaries between fundamental domains. As mentioned earlier, these subspaces are invariant under the flow for $\dot{\mathbf{x}} = \pm g(\mathbf{x})$ and are equivalent to systems of fewer than N oscillators but with possibly unequal weights w_i. With this in mind, we consider here the case of $N = 2$ oscillators with unequal weights $w_1 \neq w_2$. We find that the number of fixed points is the same as in the symmetric case, but instead of a pitchfork, there is a saddle-node (SN) bifurcation at which two additional fixed states are born. For $K \to 0^-$ the basin of attraction of the stable asynchronous state approaches the full state space T^1 in the large α limit. For $K \to 0^+$ the two stable asynchronous states approach the sync state in this limit. The attractors and bifurcations in the $K \to 0$ limit for $N = 2$, $w_1 \neq w_2$, and fixed a are shown in Fig. 2.

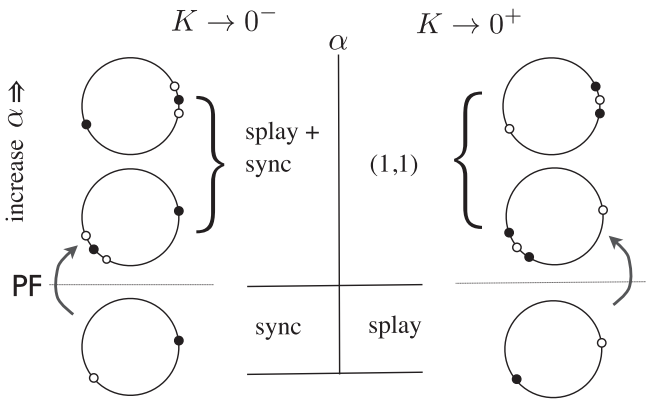

FIG. 1. The case of $N = 2$ with symmetric coupling $w_1 = w_2$: PF for $K \to 0^-$; attractors in the $K \to 0$ limit for fixed a; pitchfork bifurcation for $K \to 0^+$. (The black circles are attractors, and the white circles are repellors.)

Now we are ready to consider the system with $N = 3$ identical oscillators, which reduces to a flow on the torus T^2 ($x_3 = 0$). We represent T^2 as the unit square $0 \leqslant x_1, x_2 \leqslant 1$ with 0 and 1 identified. The diagonal $x_1 = x_2$ separates T^2 into two triangular fundamental domains with edges consisting of partially synchronized (2,1) states. The edges are invariant under the flow for $\dot{\mathbf{x}} = \pm g(\mathbf{x})$, and the dynamics on each edge is that of the $N = 2$ system with weights $\frac{1}{3}, \frac{2}{3}$, depicted in Fig. 2.

The simplest dynamics again occur for small α. The dynamics for $K \to 0^-$ on the fundamental domain $0 \leqslant x_2 \leqslant x_1 \leqslant 1$ are represented in the lower left triangle in Fig. 3. The vertices of this triangle correspond to the synchronous state, which is attracting, and the fixed point in the interior is a splay state, which is repelling. Each edge has a saddle point that is repelling along the edge. The dynamics for small α and $K \to 0^+$ have reversed flow direction, and so they have splay attracting and sync repelling. Note that the actual locations of the splay and edge saddle (ES) points are typically far from the centrally positioned points shown in Fig. 3, which is a schematic chosen to illustrate the relevant dynamical structures clearly.

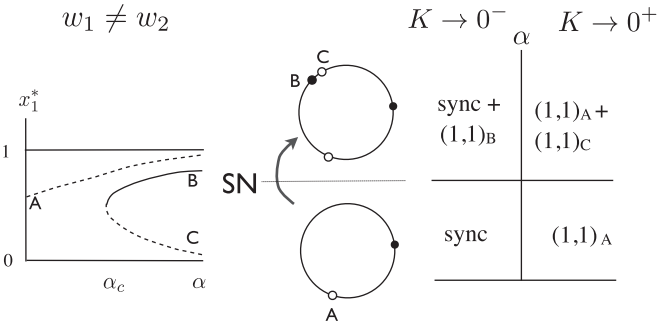

FIG. 2. The case of $N = 2$ with asymmetric coupling $w_1 \neq w_2$: bifurcation diagram for $K \to 0^-$; SN for $K \to 0^-$; attractors in the $K \to 0$ limit for fixed a.

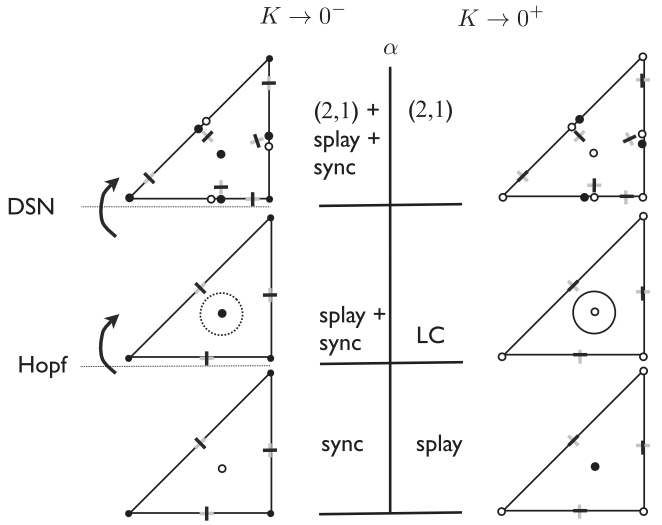

FIG. 3. $N = 3$ schematic Hopf bifurcation followed by double saddle-node (DSN) bifurcation; attractors in the $K \to 0$ limit for fixed a. (Crosses denote saddles; the darker shade indicates attracting direction.)

It is instructive to check the count of indices of all of the fixed points, which must be zero for any flow on the full state space T^2. The index of a fixed point is defined to be $(-1)^r$, where r is the dimension of the unstable manifold of the fixed point. For a two-dimensional flow, attracting and repelling fixed points have index $+1$, and saddle points have index -1. Combining this fundamental domain with its reflection in the diagonal, we see that the full state space T^2 has one sync, two splay and three saddle fixed points, which gives a total index of zero, as expected.

Upon increasing α, our numerical simulations reveal that the splay fixed point in the interior of the triangle undergoes a Hopf bifurcation at some α_H. For $K \to 0^-$ the Hopf bifurcation is subcritical, so the resulting limit cycle for $\alpha > \alpha_H$ is repelling and the splay fixed point becomes attracting. For $K \to 0^+$ the limit cycle becomes the new attractor for $\alpha > \alpha_H$ through a supercritical Hopf bifurcation.

This section has so far focused on fixed points for the $K \to 0$ limit continuous dynamical system $\dot{\mathbf{x}} = \pm g(\mathbf{x})$, which are the $K \to 0$ limits of corresponding fixed points for the discrete dynamical system defined by the return map F. Moreover, the stability behavior of the fixed points in the continuous dynamical system is also the same as that of the corresponding fixed points in the discrete system for sufficiently small $|K|$.

In contrast, when the continuous system in the limit $K \to 0$ has an attracting limit cycle, then for sufficiently small $|K| > 0$, the corresponding discrete system will exhibit the discrete analog of a limit cycle, which is a stable quasiperiodic orbit near the limit cycle. This is consistent with the quasiperiodic behavior observed numerically and attributed to a Hopf bifurcation by van Vreeswijk [7] and discussed further by Mohanty and Politi [15]. This limit cycle, however, does not exist for arbitrarily large α.

As α increases further, the LC grows until it becomes tangent to a point on each edge. Then a somewhat unusual bifurcation occurs; along each edge, the point of tangency

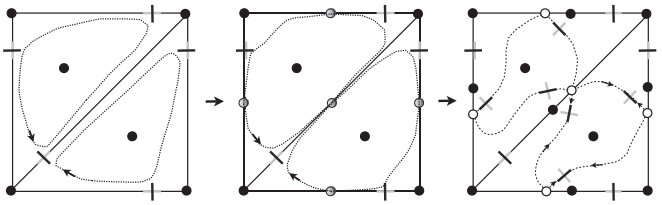

FIG. 4. Schematic of a double saddle-node bifurcation for $K \to 0^-$.

bifurcates into a sink and a source along the edge together with a pair of saddle points on either side of the edge. After this "double saddle-node" bifurcation, the remnant of the limit cycle is a heteroclinic cycle connecting the three edge sources for $K \to 0^-$ (sinks for $K \to 0^+$) and the three saddles born in the fundamental subdomain containing the limit cycle. This bifurcation is depicted in Fig. 4.

This double saddle-node bifurcation creates a new attracting fixed point on each edge; this fixed point is a partially synchronized (2,1) state. So for $K \to 0^-$, in addition to the stable sync and splay, there are now three equivalent stable partially synchronized (2,1) states for $\alpha > \alpha_{\mathrm{DSN}}$. The basins of attraction for these three types of states are illustrated in the first panel in Fig. 5. For $K \to 0^+$, the limit cycle is the only attractor for $\alpha_H < \alpha < \alpha_{\mathrm{DSN}}$, and for $\alpha > \alpha_{\mathrm{DSN}}$, the only attractors are the three equivalent stable (2,1) states born at $\alpha = \alpha_{\mathrm{DSN}}$. The basins for the three (2,1) attracting fixed points are shown in the second panel in Fig. 5. Note that the set of (2,1) states on each edge corresponds to an asymmetrically weighted $N = 2$ system, which undergoes a saddle-node bifurcation as shown in Fig. 2.

The attractors for $K \to 0$, $N = 3$, and fixed a are given in the center panel of Fig. 3. For $K \to 0^-$, both sync and splay are stable for $\alpha_H < \alpha < \alpha_{\mathrm{DSN}}$, and sync, splay, and (2,1) are stable for $\alpha_{\mathrm{DSN}} < \alpha$. The size of the sync basin (white space in the first panel of Fig. 5) vanishes in the large α limit. For $K \to 0^+$ only a single type of attractor is stable for any given α, and for $\alpha \gg \alpha_{\mathrm{DSN}}$ the stable (2,1) attractors get arbitrarily close to the unstable sync state.

For $N = 4$ the $K \to 0$ continuous dynamics have state space T^3 or equivalently the unit cube $0 \leqslant x_1, x_2, x_3 \leqslant 1$ with 0 and 1 identified ($x_4 = 0$). The dynamics for $K \to 0^-$ and small

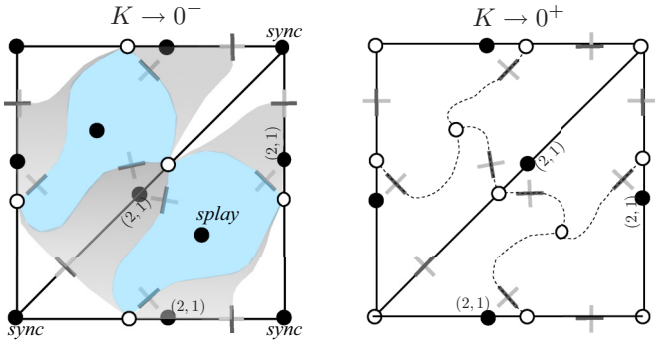

FIG. 5. The basins of attraction of the stable fixed points for large α. For $K \to 0^-$ the attractors are sync, splay, and three equivalent (2,1) states; for $K \to 0^+$ the attractors are the other three equivalent (2,1) states.

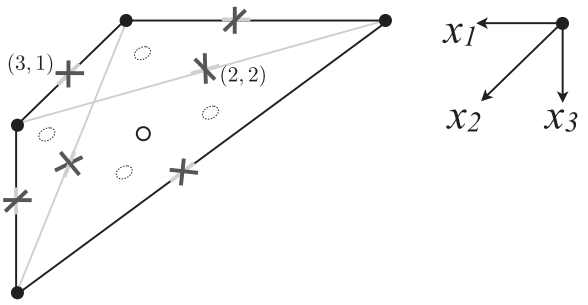

FIG. 6. $N = 4$ flow on a fundamental tetrahedral subdomain for small α and $K \to 0^-$. Partially synchronized invariant subspaces include four (3,1) edges, two (2,2) edges, and four (2,1,1) triangular faces. The broken rings indicate face saddles (FSs) that repel in the face and attract transverse to it.

α on the tetrahedral fundamental domain $0 \leqslant x_3 \leqslant x_2 \leqslant x_1 \leqslant 1$ are shown in Fig. 6. The tetrahedron's boundary has four equivalent triangular faces consisting of (2,1,1) states which are invariant under the flow for $\dot{\mathbf{x}} = \pm g(\mathbf{x})$ and correspond to the asymmetric $N = 3$ system with weights $\frac{1}{4}$, $\frac{1}{4}$, and $\frac{1}{2}$. Each face has two edges consisting of (3,1) states and one edge consisting of (2,2) states, which are drawn in a lighter shade in our figures. The full state space T^3 consists of the six fundamental subdomains generated by permutations of points (x_1,x_2,x_3) in this tetrahedron.

For $K \to 0^-$ the vertices of the tetrahedron in Fig. 6 correspond to the attracting synchronous state, and the fixed point in the interior is the repelling splay state. The saddle point on each of the six edges is repelling along the edge and has a unique attracting direction into each face. The two (2,2) edge saddles are splay (2,2) states; i.e., fixed points of the square of the single-firing map. Each of the four faces has a saddle point in its interior which is repelling in the face and attracting in the direction perpendicular to the face.

The full state space T^3 has four distinct (3,1) edges and three distinct (2,2) edges which together contain seven edge saddles (index -7); the 12 distinct faces in T^3 together contain 12 face saddles (index $+12$); and each of the six fundamental subdomains has a single splay fixed point in its interior (index -6). Together with the single sync fixed point (index $+1$), this gives a total index of zero as expected.

Since edges are invariant subspaces, a fixed point on the interior of an edge has one eigendirection along the edge. The four (3,1) edges are common to all six subdomains, and six faces meet at each (3,1) edge. So the interior saddle points on (3,1) edges have two equal eigenvalues associated with invariant two-dimensional flow transverse to the edge. There are three (2,2) edges in T^3, two of which are on the boundary of any subdomain, and four faces meet at each (2,2) edge. The interior saddle points on (2,2) edges typically have three distinct eigenvalues with eigendirections along the edge and in the two faces that meet transversely at the edge.

Upon increasing α, our numerical simulations reveal a sequence of six distinct bifurcations portrayed in Fig. 7. In the first bifurcation (labeled 22E PF) the two splay (2,2) edge saddles undergo pitchfork bifurcations that turn these splay (2,2) states into attractors and give birth to two new (2,2) edge saddle points surrounding each of the two splay (2,2) states. The new edge saddles are again repelling along the edge only.

In the second bifurcation, which creates no new attractors, two face saddles (from different subdomains) merge with each of the new (2,2) edge saddles in a reverse pitchfork bifurcation. The diagram labeled FEF rPF in Fig. 7 shows four pairs of face saddles with each pair on two parallel faces meeting at the (2,2) edge, merging with the four new (2,2) saddles in the fundamental subdomain. After this bifurcation there are no face saddles, and the (2,2) saddles are now repelling along the edges as well as the direction from which the two bifurcating saddles came. [The two (2,2) saddles surrounding an attracting splay (2,2) state are now inequivalent since their second repelling directions are orthogonal.]

Next, a limit cycle is born in a Hopf bifurcation of the interior splay fixed point as we observed for the $N = 3$ system. For $K \to 0^-$ the three repelling directions of the splay fixed point reduce to one, and the limit cycle is repelling. For

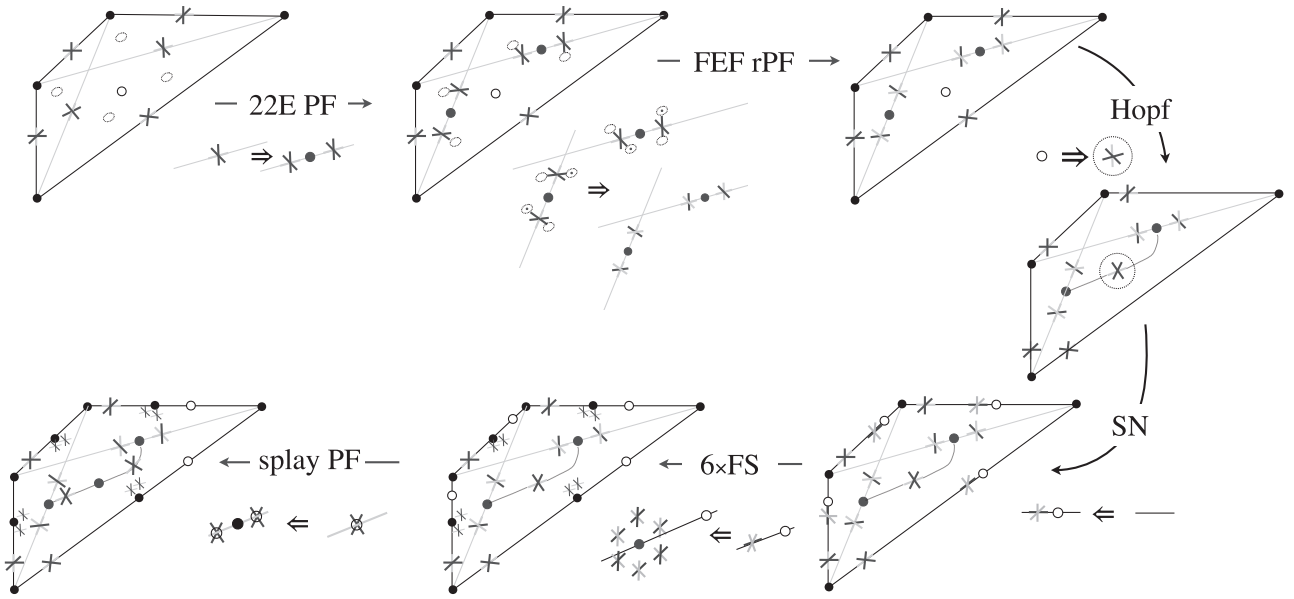

FIG. 7. Bifurcation sequence for $N = 4$ and $K \to 0^-$, starting upper left and moving clockwise.

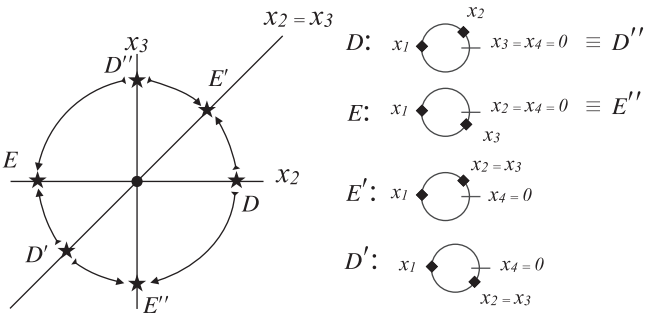

FIG. 8. Six face saddle bifurcation, viewed transverse to the (3,1) edge $0 = x_4 = x_3 = x_2 < x_1 < 1$; the center in the diagram is the edge fixed point, which is surrounded by six face saddles on the six faces meeting the edge.

$K \to 0^+$ the limit cycle is attracting, and the splay state now only has one attracting direction along which a heteroclinic orbit connects the splay with the splay (2,2) states, which are repelling for $K \to 0^+$. Note that unlike the edges, which are composed of partially synchronized states, this heteroclinic orbit is a one-dimensional invariant space in the tetrahedron's interior; and for $N = 4$ all fixed points that are not partially synchronized lie on this orbit.

The fourth bifurcation is a saddle node on each of the (3,1) edges. Upon increasing α each subdomain's limit cycle hits the (3,1) edges tangentially, and a pair of fixed points is born along each (3,1) edge. For $K \to 0^-$ one of these is a repelling source, and the other is a saddle which is attracting along the edge and repelling transverse to it.

The next bifurcation turns each of the (3,1) edge saddles born in the saddle-node bifurcation into an attractor with each simultaneously giving birth to six new face saddles on the six faces meeting a (3,1) edge. The fixed points involved in this bifurcation along the (3,1) edge $0 = x_4 = x_3 = x_2 < x_1 < 1$ are depicted in Fig. 8. The x_1^* values of the seven fixed points in this plot vary slightly, but their differences vanish at the bifurcation. The x_2^* and x_3^* values are zero, small positive, or very close to one. The central fixed point is the (3,1) edge attractor, and the six outer fixed points are the new face saddles. Although each of them has one repelling and one attracting direction within each invariant face, the sign of the eigenvalue associated with the eigendirection with a component perpendicular to each face alternates as indicated by the arrows. The D, D', and D'' face saddles are repelling away from their faces (index $+1$), whereas the E, E', and E'' face saddles are attracting toward the faces (index -1). The face saddles related by reflection about the face $x_2 = x_3$ are equivalent: $D \equiv D''$ and $E \equiv E''$. For either sign of the $K \to 0$ limit, this bifurcation leaves a sink-source pair on each (3,1) edge.

The final bifurcation is a pitchfork bifurcation of the interior splay saddle. For $K \to 0^-$, its unique negative eigenvalue changes sign making the splay state attracting, and two new interior saddles are born along a heteroclinic orbit connecting the splay state with the splay (2,2) states. For $K \to 0^+$ splay is now repelling.

The sequence of bifurcations and resulting attractors upon increasing α is summarized in Fig. 9. For $K \to 0^+$ the sequence of splay, limit cycle, and $(N-1,1)$ attractors is the

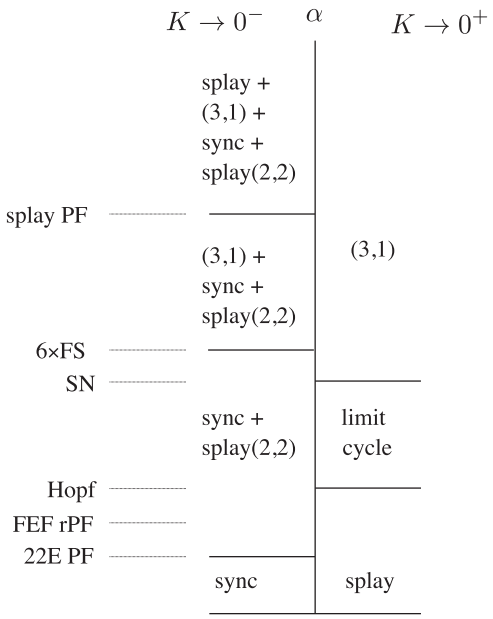

FIG. 9. The $N=4$ bifurcation sequence and resulting phase diagram, showing attractors for $K \to 0^+$ and $K \to 0^-$ for fixed a.

same as for $N = 3$. For $K \to 0^-$ the factorization $N = 4 = 2 \times 2$ supports new partially synchronized splay states, and an additional bifurcation is needed to stabilize splay.

The more exotic bifurcations we described above, namely, the double saddle node for $N = 3$ and the FEF rPF, the saddle node (with loss of limit cycles) and the 6xFS for $N = 4$ are all invariant under subgroups of the full permutation group; this property partially accounts for the nonstandard nature of these bifurcations. The properties of bifurcations under permutation symmetries are discussed in general by Ashwin *et al.* [14] and Ashwin and Swift [16].

For $N > 4$ we would expect to find even longer sequences of bifurcations that would: (i) ultimately turn the fully repelling splay state into a fully attracting state for $K \to 0^-$ and (ii) stabilize new partially synchronized splay states consistent with the prime factorization of N. For instance, for $N = 6$ we find a bifurcation sequence that first stabilizes splay (3,3) states, then splay (2,2,2) states, and ultimately fully asynchronous splay states.

V. NUMERICAL RESULTS

The bifurcation and phase diagrams discussed in the previous section are constructed based on a combination of numerical simulations, constraints associated with the hierarchy of lower-dimensional invariant subspaces in the boundaries between domains, and constraints associated with index theory for the flow on T^{N-1}. In this section we will present numerically generated examples of the dynamics for the discrete map F when $N = 3$ and $N = 4$. We simulate the dynamics by numerically solving for the time to the next spike using bisection methods and then updating $(\mathbf{x}, s, b)$ by explicitly solving the equations of motion between spikes. We use quad precision arithmetic and typically maintain accuracy to within

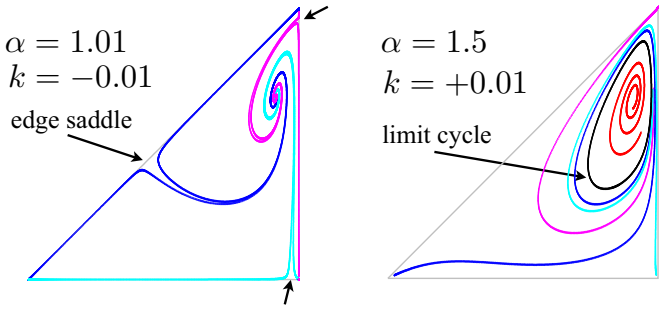

FIG. 10. Orbits for $N = 3$, $a = 1.01$, $|K| = 0.01$, and two values of α that are separated by a Hopf bifurcation and thus have different attractors; left panel: $\alpha = 1.01 < \alpha_H$, $K < 0$ and right panel: $\alpha_H < \alpha = 1.5 < \alpha_{\rm DSN}$, $K > 0$.

20 digits. For consistency we fix the parameters $a = 1.05$ and $K = +0.01$ or $K = -0.01$ and then vary α.

We first consider $N = 3$ and plot orbits (x_1,x_2) generated by iterating the map F. Starting from carefully chosen initial conditions, these orbits reveal the various saddle points and attractors shown in Fig. 3. For small but nonzero $|K|$ the orbits consist of very closely spaced discrete points. The first panel in Fig. 10 is for $\alpha = 1.01$ and $K = -0.01$. We show six orbits that all start near the splay state with two flowing to each of the triangle's vertices (which are all the same point in T^2). Pairs of orbits diverge near the three edge saddle points indicated by the arrows. The second panel is for $\alpha = 1.5$ and $K = 0.01$. The black curve is the discrete orbit approximating a limit cycle which is attracting; we also plot three orbits spiraling in toward the limit cycle, starting near each of the triangle's vertices as well as one orbit spiraling out from the splay state.

Figure 11 depicts the dynamics for $K = -0.01$ and $\alpha = 3$, after the double saddle-node bifurcation illustrated in Fig. 4. We locate the edge and face saddles by plotting carefully chosen pairs of orbits that start near the (3,1) edge sources and diverge near the various saddles. Two of these pairs of orbits diverge close to each face saddle, and one pair diverges near each edge saddle. Note that two of the face saddles lie very close to the edges and two of the edge saddles lie very close to the

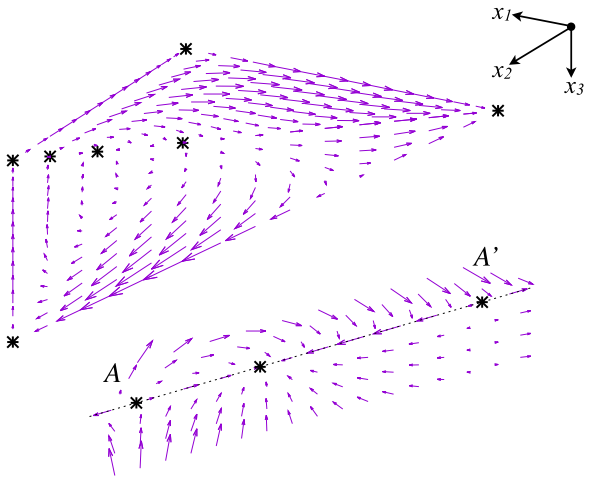

FIG. 12. Velocity field in the top ($x_3 = 0$) and side ($x_1 = x_2$) (2,1,1) faces of the tetrahedral subdomain for $\alpha = 1.133$, $a = 1.05$, and $K = -0.01$ just before the FEF-rPF bifurcation. The main panel: sync attractors at vertices plus three (2,2) edge fixed points. The inset: magnified (2,2) edge with a central splay (2,2) attractor, surrounded by two edge saddles labeled A and A'.

vertices in the main figure. The picture is clearest for the (2,1) source on the horizontal edge. From it three closely separated pairs of orbits head out to two face saddles and one edge saddle. Near the saddles, pairs of orbits diverge and approach different attractors, namely, the synchronized state at the vertices, the splay state, or one of the (2,1) edge sinks. The diverging orbits near all six saddles are magnified in the insets where orbits originating from the same source are plotted in the same color.

For $N = 4$ we present numerical results illustrating three of the six bifurcations. Although the comparison of general orbits in three dimensions (3D) is not that easy to present in figures, the new bifurcations are mostly confined to partially synchronized lower-dimensional subspaces on the fundamental domain's boundaries.

In Fig. 12 we plot data for $K = -0.01$, $a = 1.05$, and $\alpha = 1.133$ just before the FEF-rPF bifurcation that was

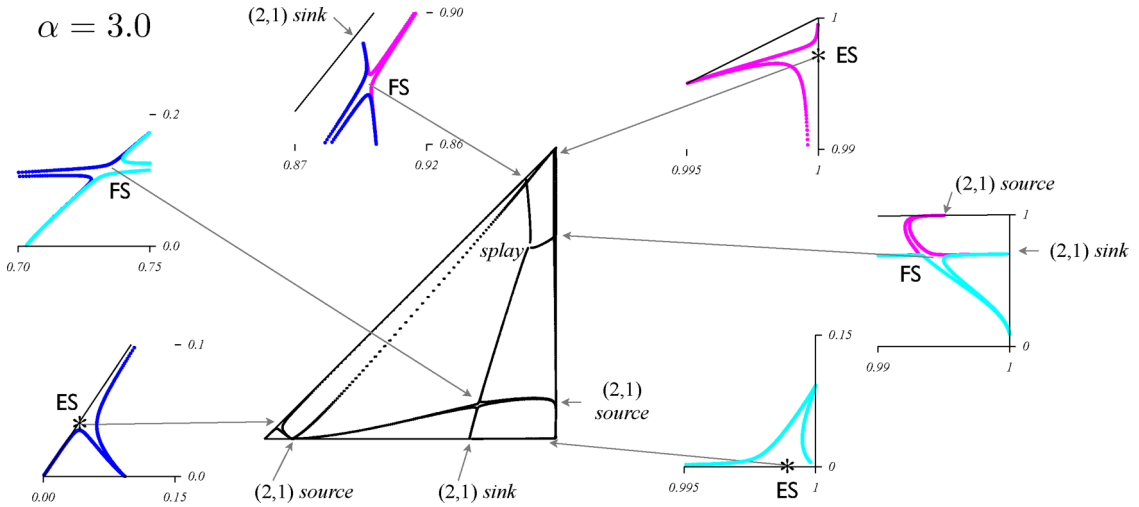

FIG. 11. Examples of orbits for $N = 3$, $a = 1.01$, $K = -0.01$, and $\alpha_{\rm DSN} < \alpha = 3$. The main panel shows pairs of orbits originating from the three (2,1) edge sources that either diverge near the FSs or near the (2,1) ESs. The orbits near each saddle are magnified in the insets.

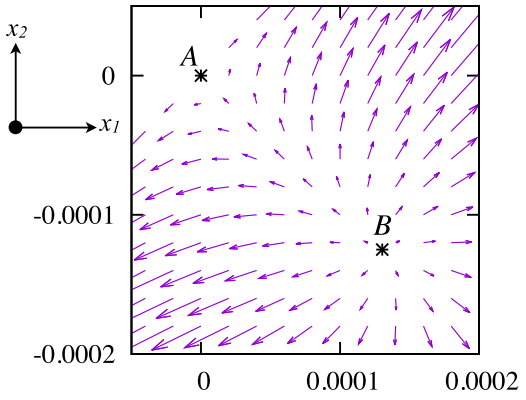

FIG. 13. Velocity field in the top ($x_3 = 0$) 211 face relative to the (2,2) edge saddle labeled A in the previous figure. At this magnification one can resolve the face saddle labeled B.

schematically represented in Fig. 7. In the main panel we show the velocity field in the top ($x_3 = 0$) and side ($x_1 = x_2$) 211 faces of the tetrahedron in Fig. 6. (Since the faces are invariant, the velocity field lies in the faces.) We indicate the fixed points at the tetrahedron's vertices corresponding to the sync attractor as well as three fixed points on the (2,2) edge which are magnified in the inset. The central fixed point on the (2,2) edge is the splay (2,2) attractor which is surrounded by two edge saddles labeled A and B. In the inset, the components of the velocity field perpendicular on the (2,2) edge as well as the vertical (x_3) component of the velocity field on the $x_1 = x_2$ face have been magnified for illustrative purposes.

In the FEF-rPF bifurcation edge saddles from parallel faces on different fundamental subdomains merge with the (2,2) edge saddles. In Fig. 13 we show the velocity relative to the (2,2) edge labeled A on the top face with sufficient magnification to also show the face saddle (which is repelling in the face) that will bifurcate with edge saddle A for slightly larger α. Here the components of the velocity field perpendicular to the (2,2) edge have been magnified 30-fold.

In Fig. 14 we plot quasiperiodic orbits for positive $K = 0.01$, $a = 1.05$, and four different values of α. The two smaller orbits for $\alpha = 1.38$ and 1.39 are composed of 420 and 430 points, respectively, each approximating one revolution of the limit cycle for $K \to 0$. The third orbit has $\alpha = 2.1$, is much

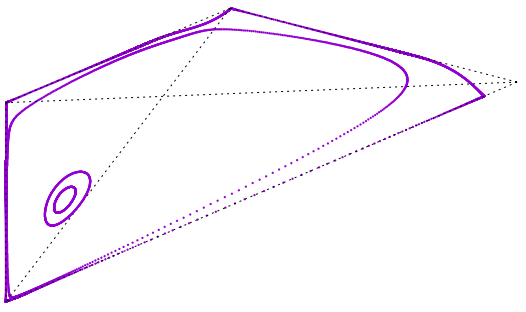

FIG. 14. Quasiperiodic orbits approximating limit cycles for positive $K = 0.01$, $a = 1.05$ for four values of α with two slightly larger than α_H ($\alpha = 1.38$ and 1.39) and two slightly smaller than α_{SN} ($\alpha = 2.1$ and 2.44). The orbits increase in size as α increases.

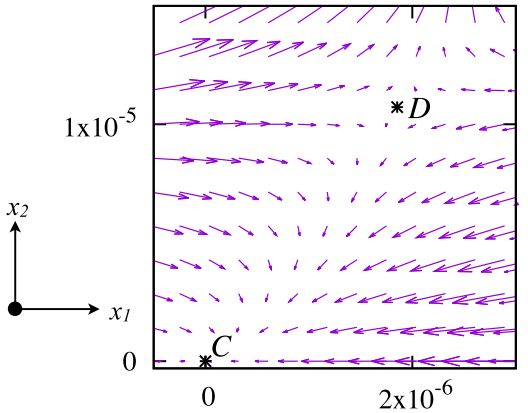

FIG. 15. Velocity field in the $x_3 = 0$ face, relative to the (3,1) attractor for $K < 0$ (labeled C) that lies on the $x_2 = 0$ edge. Here $K = -0.01$, $a = 1.05$, and $\alpha = 2.445$ which yields dynamics just after the 6xFS bifurcation that stabilizes the (3,1) attractor at the origin of the figure and in which the face saddle (labeled D) is born.

larger, and is composed of 1250 points for one approximate cycle. This orbit approaches very close to two (3,1) edges. The last orbit for $\alpha = 2.4$ is composed of 19 770 points most of which are extremely close to all four (3,1) edges. This orbit moves away from the edges near the (3,1) saddles. The orbit evolves so slowly because this value of α is very close to α_{SN}.

At α_{SN} a saddle-node bifurcation gives birth to a pair of fixed points on each (3,1) edge. For $K < 0$ one is repelling, and the other is a saddle which is attracting along the edge and repelling transverse to it. In the sixfold face saddle bifurcation, this edge saddle becomes attracting in all directions, and six face saddles are born on each of the six faces that meet each (3,1) edge as was illustrated in Fig. 8. Figure 15 shows velocity fields on the $x_3 = 0$ face, relative to the edge fixed point that is now attracting (labeled C) just after the sixfold face saddle bifurcation. The parameters are $K = -0.01$, $a = 1.05$, and $\alpha = 2.445$. The figure shows the edge attractor C and one face saddle (labeled D) on the $x_3 = 0$ face of the $x_3 < x_2 < x_1$ fundamental subdomain. To illustrate the flow, the component of the velocity field perpendicular to the horizontal edge has been magnified 5000 times.

In Figs. 13 and 15 we show velocity fields near four fixed points on the $x_3 = 0$ face. To verify our index assignment to each of these we consider the maps relating consecutive points in numerically evaluated 3D orbits near these fixed points. These maps are very close to linear, and so it is straightforward to compute the three eigenvalues of the flow near the fixed points, which are listed in Table I, as well as their eigenvectors. Note that our numerical accuracy is such that all the digits in these numbers are significant. For A and B, the eigendirection for λ_1 is transverse to the $x_3 = 0$ plane, whereas it is the eigendirection for λ_3 that is transverse to the $x_3 = 0$ plane for C and D. The (3,1) attractor C corresponds to the fixed point at the origin of Fig. 8, and its eigenvalues $\lambda_2 = \lambda_3$ correspond to flow on an invariant plane transverse to the edge. The positive λ_3 for the face saddle D implies that orbits near this fixed point but off the face flow away from this face. The table's last row lists eigenvalues for the related face saddle E on the $x_2 = x_3$ face. For it λ_3 is negative and orbits near E but off the $x_2 = x_3$

TABLE I. Eigenvalues of the four fixed points labeled A and B in Fig. 13 and C and D in Fig. 15 (which all lie on the $x_3 = 0$ face). The eigenvalues denoted by E are for the fixed point on the $x_2 = x_3$ face that is similar to D.

FP	λ_1	λ_2	λ_3
A	$-2.0805450 \times 10^{-2}$	2.881564×10^{-3}	-6.743099×10^{-5}
B	$-2.0805638 \times 10^{-2}$	2.880864×10^{-3}	6.778099×10^{-5}
C	$-1.0922055 \times 10^{-2}$	-2.429602×10^{-4}	-2.429602×10^{-4}
D	$-1.0921714 \times 10^{-2}$	2.411858×10^{-4}	2.018837×10^{-4}
E	$-1.0922258 \times 10^{-2}$	2.422949×10^{-4}	-2.322444×10^{-4}

face flow toward this face. Rotating around the (3,1) edge there are six such face saddles for which these signs of λ_3 alternate consistent with the pattern of Fig. 8.

VI. DISCUSSION

The dynamics of the pulse-coupled model with N identical oscillators studied in this paper can completely be described by a return map F on an $(N+1)$-dimensional state space. When the coupling $K = 0$, this system has an attracting invariant codimension 2 subspace on which the dynamics are purely neutral (F is the identity map on this subspace). This attracting codimension 2 invariant subspace persists for sufficiently small nonzero K, and in the $K \to 0$ limit, the dynamics to first order in K are given by a map of the form $\mathbf{x} \to \mathbf{x} + Kg(\mathbf{x})$. This discrete iteration is just Euler's method for the continuous flow $\dot{\mathbf{x}} = g(\mathbf{x})$, so in the $K \to 0$ limit the model dynamics are captured by this $(N-1)$-dimensional continuous system. Changing the sign of K corresponds to reversing the direction of this flow. The original model with N oscillators has an $(N+2)$-dimensional state space (the two extra dimensions describe the α-coupling pulse), so this achieves a reduction of three dimensions from the original model. We emphasize that the key ingredient for this reduction is the neutral dynamics for $K = 0$. We exploit this reduction in several ways; primarily, it makes it possible to depict the dynamics for as many as $N = 4$ oscillators. We also can use techniques from continuous dynamics, such as index theory, to predict the existence of various types of fixed states, especially saddles. The state space for the reduced system is stratified by a hierarchy of lower-dimensional invariant subspaces consisting of partially synchronized oscillator configurations. Except for the fully asynchronous splay states, all of the stable fixed points we found in our analysis lie on these subspaces.

In the study of oscillator networks with identical oscillators and all-to-all coupling, it is natural to focus on the stability of the fully synchronized states and their dynamical opposites, the fully asynchronous splay states (where the oscillators all have identical periodic evolution but are equally staggered in phase). These two types of states typically have natural analogs in the continuum limit ($N \to \infty$) of the model, and their stability can often be analyzed explicitly in the continuum limit. In this paper we focus on some of the other possible types of attractors for small N and find that, for the pulse-coupled model we studied, that the overall picture is much richer than a competition between sync and splay. We find many examples of stable partially synchronized attractors, such as $(N-1,1)$ fixed states, partially synchronized splay states with (2,2), (3,3), and (2,2,2) configurations, as well as stable limit cycles. This raises the possibility of a hierarchy of partially synchronized splay configurations that become stable under a sequence of bifurcations for large but finite N, depending on the prime factorization of N. These partially synchronized states do not have a well-defined analog in the continuum limit since they are dependent on the factorization of N. So we expect that in general the dynamics of our finite N model is highly dependent on N and much more intricate than that of its continuum limit analog. This certainly is the case for $N = 2$–4 where we are able to describe completely the sequence of bifurcations and all attracting states.

We have shown that the all-to-all pulse-coupled oscillator model with N identical LIF oscillators and α-function pulses can exhibit fairly intricate dynamics even for small values of N. It is natural to ask to what extent the various attractors and bifurcations we found depend on the specific details of the model or are to some degree model independent. This is an obvious direction for future exploration, although we can shed some light on this question based on some of our earlier work on Kuramoto oscillator networks [12,17]. As we mentioned in the Introduction, networks of identical Kuramoto oscillators can only have attractors that are fixed points or limit cycles, and these attracting states must be either fully synchronized or $(N-1,1)$ states. Two standard (equivalent) types of neuron models, namely, quadratic integrate-and-fire or θ-neuron models, can be transformed to the class of Kuramoto oscillators, so this remark applies to pulse-coupled networks of these types of neural models. Since the attractors must all lie in the $(N-1,1)$ subspace, it is hard to imagine a bifurcation sequence as complicated as that described in Fig. 7 for the case of identical Kuramoto networks. So we can conclude that, to at least some extent, the attractor and bifurcation structure we described depends on the details of the individual oscillator evolution.

The dynamics also depend on the details of the pulse shape. For example, the LIF model with excitatory δ-function pulses is known to synchronize for almost all initial conditions [3]. A distinguishing feature of α-function from δ-function pulses is the property that an α function peaks some time after the pulse is emitted. This feature is also present in a delayed δ-function pulse; however, as shown by Ernst *et al.* [18] and Timme *et al.* [19], synchronization is more subtle in delayed δ-function pulses, and so we would not expect a similar attractor and bifurcation structure for that model.

An important direction for future investigations that is necessary to connect to biological neural circuits is to suspend the assumption of identical oscillators. For example, one could consider a coupled LIF model with variation in the parameter a governing the evolution of the individual oscillators. For sufficiently small coupling K, the first stage of our dimensional reduction analysis goes through, giving an attracting codimension 2 invariant subspace. However the second stage of our reduction depends heavily on the assumption that the return map F, which is just the Poincaré map section, reduces to the identity map when $K = 0$. This obviously fails to hold for nonidentical oscillators, so we believe that the final reduction to a codimension 3 continuous flow is not possible in the more general setting of nonidentical oscillators. Nevertheless, with

two dimensions of reduction this model should be numerically tractable for small values of N, and we would expect it to have similar dynamics to our identical LIF model at least for sufficiently small variation in the oscillator periods. The fixed points and limit cycles in T^{N-1} discussed in this paper persist for nonidentical oscillators and correspond to limit cycles and invariant tori, respectively, in T^N just as they do for identical oscillators. These invariant tori are similar to the invariant two-dimensional surfaces we introduced in the context of periodically driven Hodgkin Huxley oscillators in Ref. [20].

ACKNOWLEDGMENTS

We thank A. Torcini for carefully reading a previous version of this paper and offering many insightful comments and suggestions. This work was partially supported by NSF Grant No. DMS 1413020.

[1] A. T. Winfree, J. Theor. Biol. **16**, 15 (1967).
[2] C. S. Peskin, *Mathematical Aspects of Heart Physiology* (Courant Institute of Mathematical Sciences, New York University, New York, 1975).
[3] R. E. Mirollo and S. H. Strogatz, SIAM J. Appl. Math. **50**, 1645 (1990).
[4] L. F. Abbott and C. van Vreeswijk, Phys. Rev. E **48**, 1483 (1993).
[5] R. Zillmer, R. Livi, A. Politi, and A. Torcini, Phys. Rev. E **74**, 036203 (2006).
[6] C. van Vreeswijk, L. F. Abbott, and G. B. Ermentrout, J. Comput. Neurosci. **1**, 313 (1994).
[7] C. van Vreeswijk, Phys. Rev. E **54**, 5522 (1996).
[8] R. Zillmer, R. Livi, A. Politi, and A. Torcini, Phys. Rev. E **76**, 046102 (2007).
[9] S. Olmi, A. Politi, and A. Torcini, J. Math. Neurosci. **2**, 12 (2012).
[10] M. Dipoppa, M. Krupa, A. Torcini, and B. S. Gutkin, SIAM J. Appl. Dyn. Syst. **11**, 864 (2012).
[11] S. Olmi, A. Torcini, and A. Politi, Front. Comput. Neurosci. **8**, 8 (2014).
[12] J. R. Engelbrecht and R. Mirollo, Chaos **24**, 013114 (2014).
[13] V. I. Arnold, *Geometrical Methods in the Theory of ODEs*, Grundlehren der mathematischen Wissenschaften Vol. 250 (Springer, Berlin, 1988).
[14] P. Ashwin, G. King, and J. W. Swift, Nonlinearity **3**, 585 (1990).
[15] P. K. Mohanty and A. Politi, J. Phys. A **39**, L415 (2006).
[16] P. Ashwin and J. Swift, J. Nonlinear Sci. **2**, 69 (1992).
[17] J. R. Engelbrecht and R. Mirollo, Phys. Rev. Lett. **109**, 034103 (2012).
[18] U. Ernst, K. Pawelzik, and T. Geisel, Phys. Rev. Lett. **74**, 1570 (1995).
[19] M. Timme, F. Wolf, and T. Geisel, Phys. Rev. Lett. **89**, 154105 (2002).
[20] J. R. Engelbrecht, K. Loncich, R. Mirollo, M. E. Hasselmo, and M. Yoshida, J. Comput. Neurosci. **34**, 59 (2013).